

Rotational spectroscopy and equilibrium structures of S_3 and S_4

S. Thorwirth,^{a)} M. C. McCarthy, C. A. Gottlieb, and P. Thaddeus
Harvard-Smithsonian Center for Astrophysics, Cambridge, Massachusetts 02138
and Division of Engineering and Applied Sciences, Harvard University, Cambridge, Massachusetts 02138

H. Gupta and J. F. Stanton
Institute for Theoretical Chemistry, Department of Chemistry and Biochemistry,
University of Texas at Austin, Austin, Texas 78712

(Received 1 April 2005; accepted 4 May 2005; published online 10 August 2005)

The sulfur molecules thiozone S_3 and tetrasulfur S_4 have been observed in a supersonic molecular beam in the centimeter-wave band by Fourier transform microwave spectroscopy, and in the millimeter- and submillimeter-wave bands in a low-pressure glow discharge. For S_3 over 150 rotational transitions between 10 and 458 GHz were measured, and for S_4 a comparable number between 6 and 271 GHz. The spectrum of S_3 is reproduced to within the measurement uncertainties by an asymmetric top Hamiltonian with three rotational and 12 centrifugal distortion constants; ten distortion constants, but an additional term to account for very small level shifts caused by interchange tunneling, are required to reproduce to comparable accuracy the spectrum of S_4 . Empirical equilibrium (r_e^{emp}) structures of S_3 and S_4 were derived from experimental rotational constants of the normal and sulfur-34 species and vibrational corrections from coupled-cluster theory calculations. Quantum chemical calculations show that interchange tunneling occurs because S_4 automerizes through a transition state with D_{2h} symmetry which lies about 500 cm^{-1} above the two equivalent C_{2v} minima on the potential energy surface. © 2005 American Institute of Physics. [DOI: 10.1063/1.1942495]

I. INTRODUCTION

The large number of allotropic forms of sulfur—exceeding that of any other element—has long stimulated the curiosity of chemists. Besides a number of chain configurations, cyclic sulfur allotropes from S_6 to S_{20} have been isolated and characterized (mostly in the solid phase) by various techniques, including x-ray diffraction and Raman and infrared spectroscopy,¹ but very little structural information has been available for small clusters except S_2 . The most stable forms of thiozone (S_3) and tetrasulfur (S_4) were recently detected here by Fourier transform microwave (FTM) spectroscopy.^{2,3} The present investigations (this work and Refs. 2 and 3) mark the first detection of S_3 and S_4 by means of high-resolution spectroscopy and the determination of precise molecular structures for both molecules.

Sulfur clusters pose challenging problems to quantum chemistry, and a large number of theoretical papers on them have appeared.⁴ For S_3 the structure with C_{2v} symmetry shown in Fig. 1 is predicted to be more stable than a cyclic D_{3h} structure by about 5–10 kcal/mol. For S_4 there is some ambiguity, since the structures and relative energies of the isomers are quite sensitive to the level of theory, and several different isomers have been calculated to be the global minimum on the potential energy surface. Recent calculations suggest that the C_{2v} structure in Fig. 1 is the most stable,^{5,6} but a rectangular D_{2h} isomer which has been found to be a transition state for interchange tunneling is only a few kcal/mol higher in energy. There is clear evidence for interchange

tunneling in S_4 in the FTM data discussed here, but it is not possible to determine the barrier height from this data alone.³

Here a joint experimental and theoretical investigation of S_3 and S_4 is presented. The new laboratory and computational work amplifies our preliminary experimental results and extends the quantum calculations to coupled clusters methods. The present paper consists of (i) a comprehensive study of the rotational spectra of S_3 and S_4 in the centimeter and submillimeter bands to frequencies as high as 458 GHz; (ii) a study of the rotational spectra of the single sulfur-34

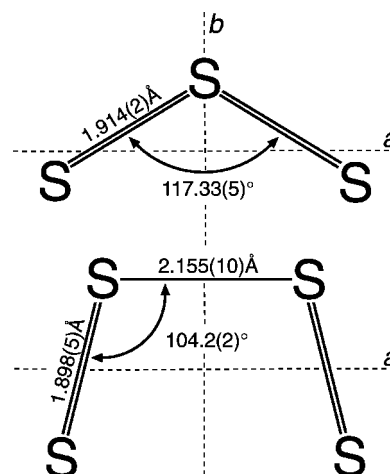


FIG. 1. Empirical equilibrium structures (r_e^{emp}) of S_3 and S_4 . Bond lengths and angles were derived from experimental rotational constants which were converted to equilibrium constants with theoretical vibration-rotation interaction constants (see Sec. V). Estimated 1σ uncertainties are given in parentheses. The bond orders are approximate.

^{a)}Electronic mail: sthorwirth@cfa.harvard.edu

isotopic species; (iii) a study of the geometrical structures, dipole moments, and vibrational energies of ground-state S_3 and S_4 ; (iv) detection of vibrational satellites belonging to S_3 and their assignment on the basis of a calculated cubic force field; and finally, (v) a theoretical investigation of the double minimum potential of S_4 .

II. EXPERIMENT

A. Centimeter-wave measurements

The FTM spectrometer used for the present work operates from 5 to 43 GHz.^{7,8} Reactive molecules are produced in the throat of a small supersonic nozzle by a low-current dc discharge through various precursor gases heavily diluted in a noble buffer gas. Free expansion from the nozzle into the large vacuum chamber of the spectrometer then forms a Mach 2 supersonic beam with a rotational temperature of only 1–3 K. Following excitation of a rotational transition by a short microwave pulse, radiation from the coherently rotating molecules is detected with a sensitive heterodyne receiver.

The initial detection of S_3 was in a discharge of hydrogen sulfide (H_2S) heavily diluted to about 0.2% in neon, chosen because H_2S is well known to be a good source of compounds such as HS_2 , H_2S_2 , and H_2S_3 .⁹ Initially, a search for the $2_{1,1}-2_{0,2}$ transition of S_3 was undertaken in a fairly wide band between 20 and 25 GHz. Assays performed on candidate lines established that a line near 21.7 GHz was only seen as a discharge product and exhibited no detectable Zeeman effect when a permanent magnet was brought near the molecular beam—as expected for a closed-shell molecule such as S_3 . This line was also present when D_2S replaced H_2S and argon replaced neon, ruling out hydrogen containing discharge products or a van der Waals complex with the buffer gas. Owing to the high signal-to-noise ratio, the corresponding lines of the two singly substituted sulfur-34 isotopic species were then found in spite of the low natural abundance of ^{34}S (4.2%). The close agreement (to better than 1%) between the observed frequency shifts for the rare isotopic species and those predicted from the structure in Fig. 1 is compelling evidence that the 21.7-GHz line is from S_3 and no other pure sulfur cluster.

Following spectroscopic identification, the production of S_3 from various precursors was investigated. Five were tested, yielding the relative line intensities and abundances in Table I. Among those which are either gases at room temperature (OCS, SO_2 , and H_2S) or a highly volatile liquid (CS_2), H_2S was found to be the best source of S_3 , presumably because its primary decomposition products are SH ($^2\Pi$) and S in its 3P ground state, formed by sequential loss of hydrogen;¹⁰ subsequent reactions of either can form small sulfur clusters and S_nH_m species, including the closely related sulfur chains HS_2 and HS_3H .⁹ Although decomposition of the other precursors tested is also known to produce atomic sulfur,¹¹ each yields much weaker lines of S_3 (by at least a factor of 10) relative to H_2S . The lower production of S_3 with these precursors may correlate with the amount of ground-state $S(^3P)$ in the discharge. In the flash photolysis of OCS, for example, nearly three-fourths of the S atoms are

TABLE I. Relative line intensities and abundances of S_3 produced from different precursors.

Precursor ^a	Relative intensity ^b	Relative abundance
H_2S	1.0	1.0
SO_2	0.1	0.1
CS_2	0.02	0.02
OCS	<0.02	<0.02
gaseous S_8	12	25 ^c

^aEach gas was heavily diluted (99–99.9%) in neon.

^bFrom measurements of the intensity of the $2_{1,1} \rightarrow 2_{0,2}$ transition at 21 679.9 MHz.

^cThe relative abundance is about two times higher than the relative intensity, owing to the higher rotational temperature of S_3 produced from gaseous S_8 in the heated nozzle ($T_{rot} \sim 4$ K) compared with that of the other precursors ($T_{rot} \sim 2$ K).

produced in the 1D excited state¹² and many collisions (roughly 20 when CO_2 is the buffer gas) are required to deactivate $S(^1D)$ to the ground state.¹³ If S_3 is formed stepwise from $S(^3P)$ and only 1/4 of the sulfur atoms are in this state, the mole fraction of S_3 may be reduced by up to a factor of roughly $(1/4)^3 = 1/64$ for OCS compared to H_2S , even if the mole fraction of S is the same.

By far the best source for S_3 was found to be a discharge through sulfur vapor (0.1%) in neon produced by flowing the neon over sulfur powder resistively heated to 185 °C (see Appendix); with a discharge voltage of 600–700 V, this arrangement yielded lines stronger by about a factor of 12 relative to those from H_2S (Table I). As an example of the high abundance of S_3 in our molecular beam, a spectrum of the $1_{1,1}-0_{0,0}$ transition of the doubly substituted sulfur-34 species $^{34}S^{34}S^{32}S$ was observed in natural abundance (0.3%) (Fig. 2). This large enhancement of S_3 over that found with other sulfur precursors suggests that in addition to sequential formation from atomic and diatomic sulfur, S_3 may be formed directly by fragmentation of S_8 .

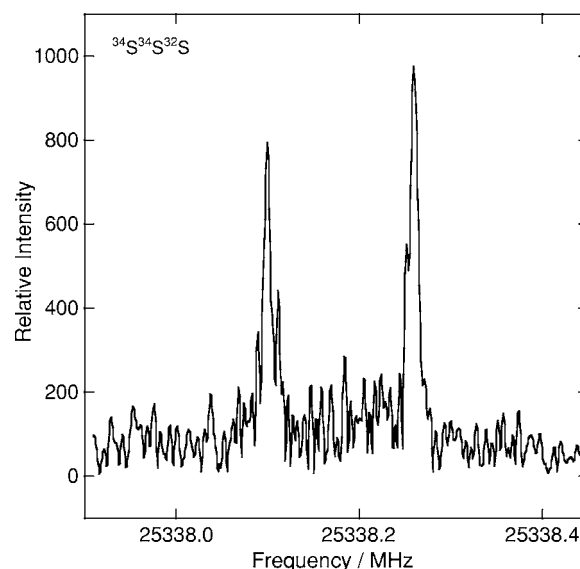


FIG. 2. The $1_{1,1}-0_{0,0}$ transition of $^{34}S^{34}S^{32}S$ at 25 338.2 MHz observed in natural abundance in a supersonic beam with an integration time of 14 min. The abundance of the doubly substituted sulfur-34 species is $\sim 3 \times 10^{-3}$ that of the normal isotopic species.

Following detection and spectroscopic characterization of S₃, a search for rotational lines of S₄ was undertaken in the sulfur vapor discharge. S₄ is predicted to be even more polar than S₃, and to have a strong rotational transition (1_{1,1}–0_{0,0}) near 6.1 GHz. A strong line near that frequency was detected which was so intense that we were able to find the two singly substituted sulfur-34 counterparts in natural abundance at almost exactly the predicted isotope shifts.

B. Millimeter-wave measurements

The millimeter-wave spectra of S₃ and S₄ were measured in absorption in a free-space glass discharge cell (1.5 m long, 7 cm in diameter) with a spectrometer described elsewhere.¹⁴ Small sulfur clusters were produced by heating elemental sulfur *in situ* in a low-pressure dc discharge through a steady stream of argon. Lines of S₃ appear when the temperature of the discharge cell (50–60 °C) is well below the melting point of sulfur. At that temperature the vapor pressure of sulfur is very low ($\ll 1$ mTorr), but the sublimation rate is fairly high.¹⁵

Spectra were recorded with the cell heated over its full length to 70 °C and carrying a discharge current of 20 mA, with an argon flow of 9 cm³/min at STP, and a total pressure (with the discharge on) of 45 mTorr. Lines of S₃ were then quite strong: for example, near 350 GHz, a signal-to-noise ratio $S/N > 100$ could be achieved with an integration time of less than 5 min. Although the dipole moment (the dipole moments calculated at the CCSD(T)/cc-pVTZ level of theory are 0.51 D for S₃ and 1.15 D for S₄) of S₄ is 2.3 times larger than that of S₃, lines of S₄ observed in the same discharge were roughly ten times weaker than those of S₃ because the rotational and the vibrational partition functions are 3.5 times larger than that of S₃, and the mole fraction of S₄ (2×10^{-4}) is 4.5 times smaller than that of S₃ (9×10^{-4}). Further increase in the intensity of the S₃ lines was observed when the temperature was raised still higher to 90–95 °C, but the discharge then became unstable, to the point that good spectra could not be obtained.

At 70 °C sulfur vapor consists almost entirely of S₈, but Hassanzadeh and Andrews¹⁶ showed that S and S₂ are produced at that temperature in a discharge very similar to ours (see Fig. 1 in Ref. 17). We were unable to observe atomic S because the lowest-frequency fine-structure transition (³P₁–³P₀) is in the far IR at 5.3 THz, but we have observed fairly intense spectra of three magnetic dipole transitions of S₂: (*N*,*J*)=(13,13–13,12) at 163.6 GHz, (15,15–15,14) at 178.4 GHz, and (17,17–17,16) at 191.3 GHz. From these spectra we estimate a mole fraction of S₂ of ~ 0.01 , implying that (i) roughly 10% of the S₈ in the vapor phase is converted to S₂ in the discharge, and (ii) the mole fraction of S₂ is ten times higher than that of S₃ and 50 times higher than that of S₄.

Intense lines of S₂O and SO₂ were also observed when the concentrations of S₃ and S₄ in the glow discharge were high. The mole fraction of S₂O was only five times less than that of S₃, probably because of residual sources of oxygen in the absorption cell. Rotational lines were readily identified

for SO₂ by consulting the standard spectral line catalog,¹⁸ and for S₂O from predictions based on published measurements.¹⁹

III. QUANTUM CHEMICAL CALCULATIONS

The structural parameters of S₃ and S₄ required to interpret the present laboratory spectroscopic data were calculated with coupled-cluster theory,²⁰ and the correlation-consistent basis sets of Dunning.²¹ Equilibrium geometries were obtained with the CCSD(T) treatment of correlation²² and the cc-pVTZ basis set using analytical energy derivatives.²³ Anharmonic force fields were calculated by numerical differentiation of analytic second derivatives²⁴ evaluated at points displaced from equilibrium along the dimensionless normal coordinates defined by the quadratic force field. Details of this procedure are given in Ref. 25. The anharmonic force fields for S₃ and S₄ were then used in conjunction with standard rovibrational perturbation theory²⁶ to calculate the fundamental vibrational frequencies and vibration-rotation interaction constants $\alpha_i^{A,B,C}$.

To investigate the fluxional nature of S₄, which automerizes through a transition state with *D*_{2h} symmetry, further calculations were undertaken. First, the *D*_{2h} structure was optimized with CCSD(T) and the cc-pVTZ basis set to estimate the barrier height. Additional calculations were carried out to study the pathway for automerization. In these, the S–S–S angle was varied over a grid of points and the remaining structural parameters optimized using analytic derivatives.

All calculations reported in this work were performed with a local version of the ACES II program system.²⁷ The treatment of correlation included all electrons in the evaluation of the molecular parameters (equilibrium structures, vibrational frequencies, and vibration-rotation interaction constants); only the valence electrons were correlated in the more qualitative exploration of the S₄ automerization potential.

IV. RESULTS

Both S₃ and S₄ have *C*_{2v} symmetry (Fig. 1) in the isomers calculated to be most stable at the highest level of theory studied.⁴ The rotational spectra are those of a nearly prolate (S₃) or somewhat prolate (S₄) asymmetric top ($\kappa = -0.97$ and -0.54 , respectively), with *b*-type transitions and Bose–Einstein statistics. As a result, the allowed rotational levels are those that are even upon nuclear permutations (i.e., with $K_a K_c = ee$ or oo)—a restriction relaxed in the singly substituted isotopic species where the *C*_{2v} symmetry is broken.

A. Thiozone, S₃

1. Rotational spectrum

With the FTM spectrometer, 17 lines of the main isotopic species of S₃ with $J \leq 12$ and $K_a \leq 2$ were measured in the centimeter-wave band between 9 and 40 GHz [see Table I of supplementary material (SM), deposited in the Electronic Physics Auxiliary Publication Service (EPAPS) of the

TABLE II. Spectroscopic constants of thiozone, S₃ (in MHz).

Constant ^a	³² S ₃		S ³⁴ SS	³⁴ SS ₂
	Measured ^b	Theoretical ^c	Measured ^d	Measured ^d
<i>A</i>	23 972.5807(4)	23 159.	23 033.906(2)	23 738.354(2)
<i>B</i>	2948.546 79(7)	2885.	2948.6856(6)	2861.0127(4)
<i>C</i>	2622.291 12(7)	2562.	2610.6946(5)	2550.1327(4)
10 ³ <i>D_J</i>	0.799 67(3)	0.77	0.79(1)	0.754(8)
10 ³ <i>D_{JK}</i>	-20.279(1)	-19.	-19.1(2)	-19.7(2)
<i>D_K</i>	0.503 44(1)	0.45	0.503 ^e	0.503 ^e
10 ³ <i>d₁</i>	-0.163 171(7)	-0.16	-0.167(3)	-0.151(2)
10 ⁶ <i>d₂</i>	-7.232(4)	-6.6	-7.23 ^e	-7.23 ^e
10 ⁹ <i>H_J</i>	0.460(4)			
10 ⁹ <i>H_{JK}</i>	-9.17(9)			
10 ⁶ <i>H_{KJ}</i>	-1.59(1)			
10 ³ <i>H_K</i>	0.034 02(8)			
10 ⁹ <i>h₁</i>	0.216(1)			
10 ⁹ <i>h₂</i>	0.0242(9)			
10 ¹² <i>h₃</i>	6.1(2)			
Δ ^f	0.243		0.248	0.245

^aThe 1σ uncertainties (in parentheses) are in the units of the last significant digits.

^bDerived from a least-squares fit of Watson's *S*-reduced Hamiltonian to the data in Table I of SM (Ref. 28).

^cCalculated at the CCSD(T)/cc-pVTZ level of theory.

^dDerived from a least-squares fit of Watson's *S*-reduced Hamiltonian to the data in Table II of SM (Ref. 28).

^eConstrained to value derived for the normal isotopic species.

^fInertial defect, Δ = *I_c* - *I_a* - *I_b*, in units of amu Å².

American Institute of Physics].²⁸ These were reproduced to within the measurement uncertainties (2–5 kHz) with eight spectroscopic constants in Watson's *S*-reduced Hamiltonian: three rotational and five fourth-order centrifugal distortion constants. Two singly substituted sulfur-34 species were also investigated: nine lines for S ³⁴SS and 16 lines for ³⁴SSS, including previously forbidden transitions now allowed by the broken symmetry [Table II of SM (Ref. 28)]. For both species, only three of the five fourth-order distortion constants (*D_J*, *D_{JK}*, and *d₁*) were determined (*D_K* and *d₂* were constrained to the values for the normal species).

To better determine the centrifugal distortion, S₃ was then studied in the millimeter- and submillimeter-wave bands. The first lines observed were series of *R*-branch transitions with low *K_a* in the region of 170–191 GHz, found

TABLE III. Rotational constants of S₃ in the ν₁ vibrational mode (in MHz).

Vibrational state	Constant ^a			
	<i>A</i>	<i>B</i>	<i>C</i>	Δ ^b
1 ν ₁	24 015.954	2938.279	2611.552	0.475
2 ν ₁	24 059.681	2928.031	2600.944	0.700
3 ν ₁	24 103.706	2917.801	2590.461	0.920
4 ν ₁	24 147.964	2907.595	2580.096	1.134
5 ν ₁	24 192.353	2897.408	2569.844	1.343
6 ν ₁	24 236.735	2887.243	2559.697	1.547
7 ν ₁	24 280.914	2877.101	2549.650	1.746

^aRotational constants derived from a least-squares fit of Watson's *S*-reduced Hamiltonian to the data in Table III of SM (Ref. 28) with centrifugal distortion constants constrained to those in the ground vibrational state (see Table II).

^bThe inertial defect, Δ = *I_c* - *I_a* - *I_b*, in units of amu Å².

within a few megahertz of predictions based on the FTM data. In all, 152 lines of S₃ with *J* ≤ 87 and *K_a* ≤ 12 were measured at frequencies as high as 458 GHz [Table 1 of SM (Ref. 28)], allowing the determination of all seven sixth-order centrifugal distortion constants. The rotational and centrifugal distortion constants of S₃ are given in Table II.

2. Vibrational excitation

Although rotational cooling to only a few kelvin is achieved in our molecular beam, vibrational cooling is much less efficient, and rotational lines in vibrationally excited states (vibrational satellites) are frequently observed in FTM

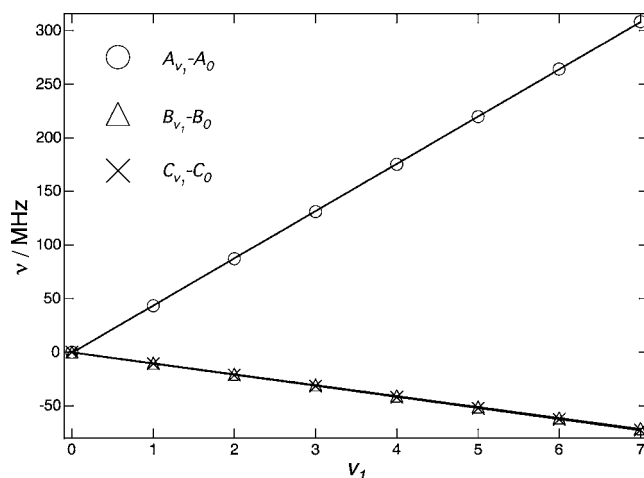


FIG. 3. Differences in rotational constants of S₃ in the ground and the vibrationally excited levels of the ν₁ mode vs vibrational quantum ν₁. Experimental values for α₁^A, α₁^B, and α₁^C determined from the slopes are in very good agreement with those calculated theoretically (see Sec. IV A 2).

TABLE IV. Theoretical vibration-rotation interaction constants of S₃ (in MHz) calculated at the CCSD(T)/cc-pVTZ level of theory.

Vib. mode and $\Sigma_i \alpha_i/2$	SSS		
	α_i^A	α_i^B	α_i^C
ν_1	-47.06	+9.93	+10.34
ν_2	-242.73	-0.60	+2.42
ν_3	+199.66	+7.59	+6.18
$\Sigma_i \alpha_i/2$	-45.07	+8.46	+9.47
	³⁴ SSS		
	α_i^A	α_i^B	α_i^C
ν_1	-48.87	+9.58	+10.00
ν_2	-236.40	-0.59	+2.27
ν_3	+197.18	+7.31	+5.98
$\Sigma_i \alpha_i/2$	-44.04	+8.15	+9.12
	S ³⁴ SS		
	α_i^A	α_i^B	α_i^C
ν_1	-38.90	+9.74	+10.09
ν_2	-233.85	-0.57	+2.51
ν_3	+186.51	+7.46	+6.05
$\Sigma_i \alpha_i/2$	-43.12	+8.32	+9.32

experiments.²⁹ Vibrational satellites up to $\nu=7$ were observed for several rotational transitions of the normal species of S₃ [Table III of SM (Ref. 28)], and from these sets of rotational constants were determined (Table III).

The vibrational dependence of the difference in the rotational constants in the vibrationally excited states (Table III) and those in the ground state satisfy the well-known relation

$$B_\nu - B_0 = -\nu \alpha_i^B, \quad (1)$$

with analogous equations for the A and C rotational constants. The experimental vibration-rotation interaction constants $\alpha_i^{A,B,C}$ for a particular vibrational state were obtained from linear fits to the differences ($A_\nu - A_0$, $B_\nu - B_0$, and $C_\nu - C_0$) as a function of the vibrational quantum number ν (Fig. 3), yielding the values $\alpha^A = -44.1$ MHz, $\alpha^B = 10.2$ MHz, and $\alpha^C = 10.4$ MHz, with estimated 1σ uncertainties of 0.1 MHz. A comparison of these experimental vibration-rotation interaction constants with those obtained theoretically (Table IV) shows that the observed vibrational

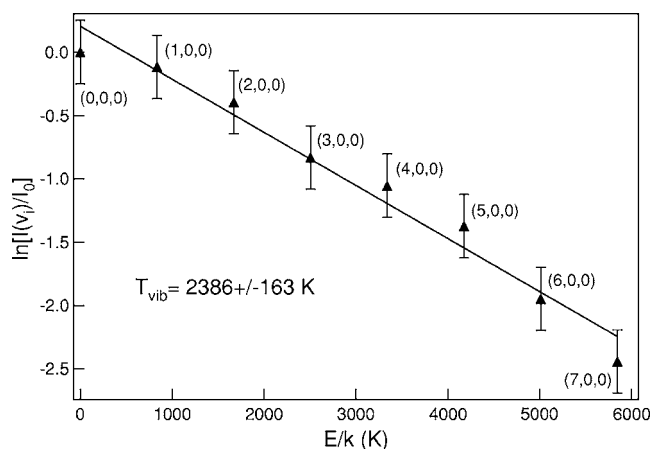


FIG. 4. Vibrational temperature diagram for the ν_1 mode of S₃ in our supersonic beam. Relative intensities in the vibrational levels [$I(\nu_i)/I_0$] are from measurements of the $1_{1,1}-2_{0,2}$ transition observed here in a discharge through sulfur vapor with the FTM spectrometer.

satellites almost certainly arise from the symmetric stretching mode ν_1 calculated to lie at 580 cm^{-1} (Table V). The close agreement of the theoretical interaction constants with the experimental values (to 7% or better) confirms that the theoretical potential surface provides a fairly good description of the vibrational dependence of the rotational constants (see Sec. V).

The vibrational temperature of the ν_1 mode of S₃ was determined from a fit of the relative intensities of the $1_{1,1}-2_{0,2}$ line in different levels with respect to the ground state on the assumption of a Boltzmann distribution. From these measurements an effective vibrational temperature of 2400 ± 160 K was found (Fig. 4). Detection of the ν_1 mode but not ν_2 near 255 cm^{-1} is consistent with previous studies of vibrational excitation of polyatomic molecules in our discharge nozzle which showed that vibrational levels whose frequencies are greater than kT ($\sim 450\text{ cm}^{-1}$) are little cooled in the supersonic expansion.²⁹ The ν_3 mode of S₃ near 670 cm^{-1} (Table V) was not investigated here.

B. Tetrasulfur, S₄

Eighty-four lines of all sulfur-32 S₄ with $J \leq 12$ and $K_a \leq 6$ have been measured in the centimeter-wave band from 6 to 39 GHz [Table IV of SM (Ref. 28)]. Because the A rotational constant of S₄ is five times smaller than that of S₃ (4.7 GHz versus 24 GHz) and single isotopic substitution

TABLE V. Vibrational frequencies of S₃ (in cm^{-1}).

Vib. Mode	Symmetry	Frequency ^a		Experiment	
		Harmonic	Fundamental ^b	Gas ^c	Matrix ^d
ν_1	a_1	585	580	581	581–585
ν_2	a_1	256	255	281	...
ν_3	b_1	681	671	...	676–680

^aCalculated at the CCSD(T)/cc-pVTZ level of theory (see Sec. III).

^bIncludes anharmonic contributions.

^cFrom gas-phase Raman spectroscopy (Ref. 30).

^dFrom infrared matrix isolation spectroscopy (Ref. 17).

TABLE VI. Spectroscopic constants of tetrasulfur, S₄ (in MHz).

Constant ^a	³² S ₄		³⁴ SS ₃ Measured ^d	S ³⁴ SS ₂ Measured ^e
	Measured ^b	Theoretical ^c		
<i>A</i>	4655.333 65(6)	4525.	4587.4305(2)	4586.5206(2)
<i>B</i>	2221.538 96(5)	2213.	2176.3209(2)	2198.8733(2)
<i>C</i>	1502.378 80(3)	1485.	1474.59812(7)	1484.83185(7)
10 ³ <i>D_J</i>	0.8742(2)	0.88	0.862(1)	0.833(1)
10 ³ <i>D_{JK}</i>	-1.882(1)	-1.9	-1.894(6)	-1.751(6)
10 ³ <i>D_K</i>	3.047(2)	2.8	3.00(1)	2.90(1)
10 ³ <i>d₁</i>	-0.3413(1)	-0.35	-0.3357(9)	-0.3263(10)
10 ³ <i>d₂</i>	-0.035 34(4)	-0.036	-0.0345(3)	-0.0343(4)
10 ⁹ <i>H_J</i>	-1.13(4)			
10 ⁹ <i>H_{JK}</i>	9.3(4)			
10 ⁶ <i>H_{KJ}</i>	-0.027(1)			
10 ⁶ <i>H_K</i>	0.028(2)			
10 ⁹ <i>h₁</i>	-0.48(2)			
10 ³ Δ <i>E</i> ^f	14.1(2)			
Δ ^g	0.336		0.340	0.338

^aThe 1σ uncertainties (in parentheses) are in the units of the last significant digits.

^bDerived from a least-squares fit of Watson's *S*-reduced Hamiltonian to the data in Table IV of SM (Ref. 28).

^cCalculated at the CCSD(T)/cc-pVTZ level of theory.

^dDerived from a least-squares fit of Watson's *S*-reduced Hamiltonian to the data in Table V of SM (Ref. 28).

^eDerived from a least-squares fit of Watson's *S*-reduced Hamiltonian to the data in Table VI of SM (Ref. 28).

^fEnergy term that accounts for interchange tunneling.

^gInertial defect, Δ=*I_c*−*I_b*−*I_a*, in units of amu Å².

breaks the *C*_{2*v*} symmetry, a fairly large number of lines of the singly substituted sulfur-34 species were also observed: 69 for ³⁴SS₃ [Table V of SM (Ref. 28)] and 70 for S ³⁴SSS [Table VI of SM (Ref. 28)]. When the transition frequencies of the rare isotopic species were analyzed, again with Watson's *S*-reduced Hamiltonian, including the full set of quartic centrifugal distortion constants, the rms of the fits was comparable to the measurement uncertainties (Table VI). The same fitting procedure was less successful when applied to the parent species, where a rms residual of about 14 kHz was found.³ Further analysis showed that the residuals exhibited a bimodal distribution: the *K_aK_c*=*ee*→*oo* transitions were systematically displaced from the *oo*→*ee* transitions by almost 15 kHz (see Fig. 5)—much more than the measurement uncertainty of a few kilohertz. Inclusion of a term in the Hamiltonian to account for interchange tunneling (Δ*E*=*O*⁺−*O*[−]),

however, reduced the rms error of the fit to about 1 kHz (Fig. 5), comparable to that found for the singly substituted sulfur-34 species, and yielding a precise value of the interchange tunneling frequency: 14.1±0.2 kHz. A similar effect is observed in the rotational spectrum of Ar−SO₂, where the tunneling frequency is more than 10⁴ times larger.³¹ The tunneling frequency observed here for S₄ is roughly seven orders of magnitude smaller than the ammonia inversion frequency, and is near the limit of what is now currently resolvable with our spectrometer. No smaller tunneling splitting to our knowledge has yet been observed.

The origin of the interchange tunneling in S₄ is apparent from quantum chemical calculations, which show that there are two equivalent accessible minima on the potential-energy surface that differ only in the identity of the *inner* and *outer* sulfur atoms (see Fig. 3 in Ref. 3). Between these two trap-

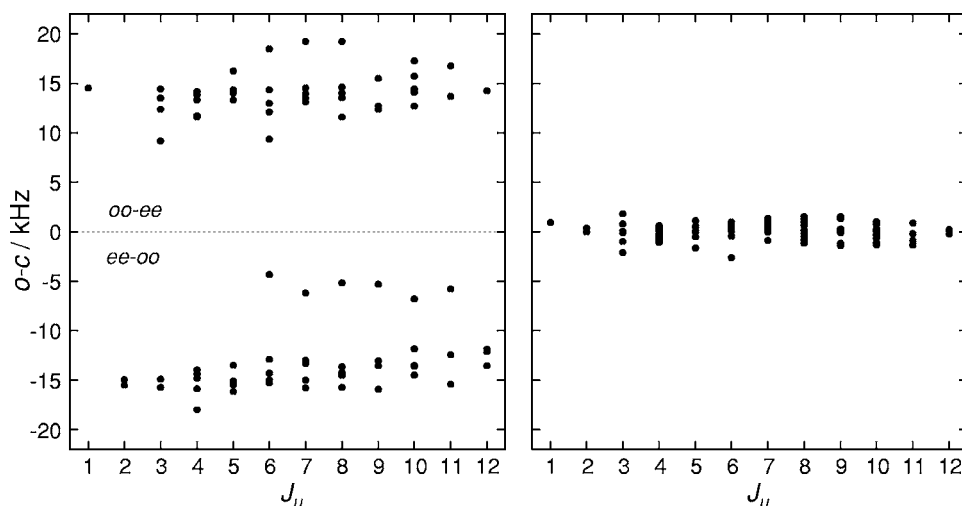


FIG. 5. Observed minus calculated frequencies (*O*−*C*) vs *J_{upper}* from a least-squares fit to the centimeter-wave measurements of S₄. Left: The residuals fall into two distinct groups depending on whether the transition corresponds to *K_aK_c*=*oo*→*ee* or *ee*→*oo*. Right: The rms of the fit (1 kHz) is comparable to the measurement uncertainties when a term that accounts for interchange tunneling (Δ*E*_{*O*⁺−*O*[−]}) is included in the Hamiltonian.

ezoidal C_{2v} structures is a rectangular D_{2h} transition state located about 500 cm^{-1} above the two equivalent minima. Using three-dimensional models of the potential-energy surface governing the tunneling motion that differ only slightly in the details of the parametrization, ground-state tunneling frequencies of about $1\text{--}100\text{ kHz}$ were obtained that are comparable to the observed frequency.

Following the FTM study of S₄, measurements were extended in the millimeter-wave band up to 271 GHz . Initially, R -branch transitions with low K_a in the range between 145 and 188 GHz were observed within a few megahertz of predictions from the centimeter-wave data. Assignment of the millimeter-wave spectrum of S₄ was more difficult than that of S₃ because lines were weaker, and there was occasional confusion with background lines, possibly the result of vibrationally excited S₃ and S₄. In all, 147 lines of S₄ were measured [Table IV of SM (Ref. 28)], yielding the spectroscopic constants in Table VI. The full set of fourth-order and five sixth-order centrifugal distortion constants were needed to adequately reproduce the measurements.

V. STRUCTURES OF S₃ AND S₄

Experimental (r_0) structures of S₃ and S₄ obtained by least-squares adjustment of bond lengths and angles to the observed rotational constants (A_0 , B_0 , and C_0) for three isotopic species were reported in preliminary accounts of this work.^{2,3} In the present investigation, the structural determination is extended to the equilibrium (r_e) structure that corresponds to the minimum on the potential-energy surface. To this end, the equilibrium rotational constants B_e are estimated from the expression

$$B_e = B_0 + \frac{1}{2} \sum_i \alpha_i^B, \quad (2)$$

where B_0 is the measured rotational constant in the ground vibrational state; similar equations hold for A_e and C_e , and the sum over vibration-rotation interaction constants is taken over each of the normal modes of vibration. The experimental determination of all the $\alpha_i^{A,B,C}$ is increasingly difficult for large molecules, but these terms can be calculated theoretically to adequate accuracy. While the vibration-rotation interaction constants (α_i) are often complicated by Coriolis and Fermi resonances, the difference between the equilibrium rotational constants and those of the ground vibrational state is determined by the sum ($\sum_i \alpha_i/2$) which is not affected by these resonance interactions within second-order perturbation theory (see Ref. 32 and references therein). This procedure of combining experimental rotational constants with theoretical vibrational corrections is generally an efficient way to determine accurate equilibrium geometries of polyatomic molecules (for a review see Ref. 33). The equilibrium structures are derived by the same least-squares fitting procedure used for the r_0 geometries, except that the equilibrium constants obtained from Eq. (2) are used instead of the experimental constants. The vibration-rotation interaction constants and the sum ($\sum_i \alpha_i/2$) for S₃ and S₄ calculated at the CCSD(T)/cc-pVTZ level of theory are given in Tables IV and VII.

TABLE VII. Theoretical vibration-rotation interaction constants of S₄ (in MHz) calculated at the CCSD(T)/cc-pVTZ level of theory.

Vib. Mode and $\sum_i \alpha_i/2$	SSSS		
	α_i^A	α_i^B	α_i^C
ν_1	+8.25	+5.50	+3.21
ν_2	+18.27	-7.44	-38.05
ν_3	-8.88	+8.73	+3.12
ν_4	+0.01	+5.79	+2.35
ν_5	+11.79	+3.07	+2.66
ν_6	-6.28	+2.25	+40.43
$\sum_i \alpha_i/2$	+11.58	+8.96	+6.86
	³⁴ SSSS		
	α_i^A	α_i^B	α_i^C
ν_1	+8.15	+5.43	+3.18
ν_2	+16.94	-7.33	-18.53
ν_3	-8.67	+8.19	+2.98
ν_4	0.00	+5.90	+2.34
ν_5	+11.46	+3.03	+2.59
ν_6	-4.80	+1.60	+20.57
$\sum_i \alpha_i/2$	+11.53	+8.41	+6.57
	S ³⁴ SSS		
	α_i^A	α_i^B	α_i^C
ν_1	+8.05	+5.26	+3.08
ν_2	+6.99	-2.76	-13.24
ν_3	-8.67	+8.87	+3.11
ν_4	+0.02	+5.41	+2.25
ν_5	+11.55	+3.04	+2.62
ν_6	+4.30	-1.64	+15.84
$\sum_i \alpha_i/2$	+11.12	+9.09	+6.83

A. S₃

For S₃, the bond length and angle are nearly the same for the experimental (r_0) and the empirical equilibrium (r_e^{emp}) structures (Table VIII), probably owing to little vibrational anharmonicity (see Table V for a comparison of the calculated fundamental and harmonic vibrational frequencies). Although the structure remains essentially unchanged when the rotational constants are corrected for vibrational effects, the inertial defects ($\Delta = I_c - I_a - I_b$) derived from the measured ro-

TABLE VIII. Structures of S₃ and S₄.

Structure ^a	S ₃		S ₄		
	$r(\text{S}=\text{S})$ (Å)	α (deg)	$r(\text{S}=\text{S})$ outer (Å)	$r(\text{S}-\text{S})$ inner (Å)	α (deg)
r_0	1.917(1)	117.36(6)	1.899(7)	2.173(32)	103.9(3)
r_e^{calc}	1.938	117.0	1.920	2.177	103.6
Recommended structure:					
r_e^{emp}	1.914(2)	117.33(5)	1.898(5)	2.155(10)	104.2(2)

^aExperimental (r_0) structures are from Refs. 2 and 3. Theoretical equilibrium (r_e^{calc}) structures were calculated at the CCSD(T)/cc-pVTZ level of theory. Empirical equilibrium (r_e^{emp}) structures were determined by the method described in Sec. V.

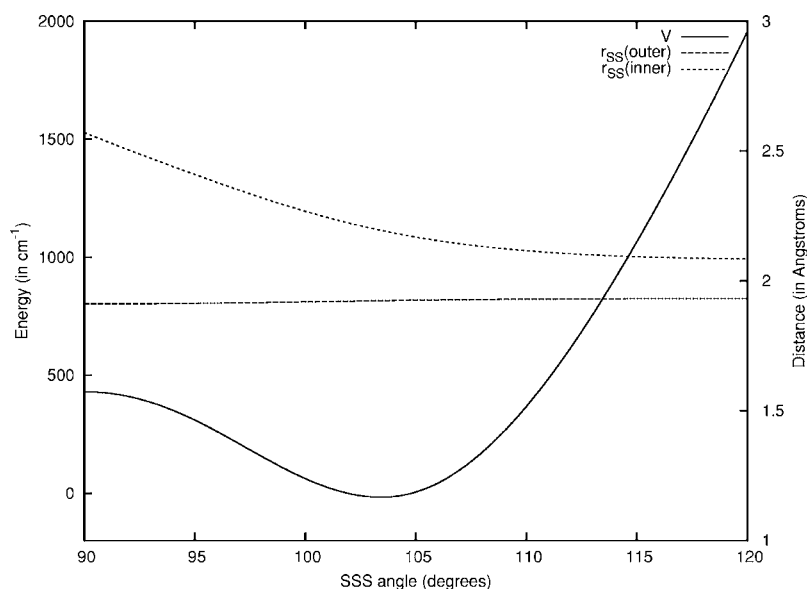


FIG. 6. Potential energy and geometrical parameters associated with the interconversion of $^4\text{SSSS}$ and S^4SSS via a D_{2h} transition state. The ordinate is the SSS bond angle, along which the other two geometrical parameters (the SS bond lengths) are optimized at each point. Calculations were performed in the frozen-core approximation at the CCSD(T)/cc-pVTZ level of theory.

tational constants for the three isotopic species, all $\sim 0.24 \text{ amu } \text{\AA}^2$, are roughly two orders of magnitude smaller for the empirical equilibrium structure (-0.005 to $-0.001 \text{ amu } \text{\AA}^2$). This large reduction in Δ , which vanishes for a rigid planar molecule, indicates that the calculated quadratic and cubic force constants for S_3 are fairly accurate.

The bond length in the theoretical equilibrium (r_e^{calc}) structure calculated at the CCSD(T) level with the cc-pVTZ basis set (1.938 Å) is about 0.02 Å longer than the experimental value (Table VIII). Experience has shown that basis set expansion tends to reduce internuclear distances while correlation tends to increase them. In the example of S_3 , the CCSD(T) method provides an adequate treatment of correlation; the major shortcoming of the calculation is the cc-pVTZ basis set. One would expect that the equilibrium bond length calculated with the cc-pVTZ basis set would be slightly on the high side, and that is what is observed for S_3 . In a similar calculation but with a more complete basis set (cc-pCVQZ), the calculated bond length (1.913 Å) is in nearly perfect agreement with that of the r_e^{emp} structure,³⁴ confirming that the calculation of the theoretical (r_e^{calc}) structure is limited by the cc-pVTZ basis set.

B. S_4

The empirical equilibrium geometry (r_e^{emp}) of S_4 was obtained as for S_3 . The central (inner) SS distance in the r_0 and r_e^{emp} structures differ by 0.02 Å, while the outer distance and the SSS bond angle are the same to within the estimated uncertainties (Table VIII). Discrepancies between the r_e^{emp} and r_e^{calc} structures for S_4 are qualitatively similar to those noted for S_3 (see Table VIII). On the assumption that the r_0 structure approximates the vibrationally averaged structure in the ground vibrational state, this difference in the inner distance in the r_0 and r_e^{emp} structures is attributed to the coupling of the stretching motion of the inner S atoms to the tunneling coordinate (here taken as the SSS bond angle θ), where θ is 90° at the transition state and θ_e is roughly 105° at the equilibrium geometry. The shape of the potential for the bending motion (Fig. 6) implies that the ground state wave

function is greater at angles less than θ_e where the S–S distance is longer, than at $\theta > \theta_e$ where the distance is shorter than r_e .

The inertial defect derived from the empirical equilibrium structure of S_4 ($\leq -0.01 \text{ amu } \text{\AA}^2$) is more than an order of magnitude smaller than that derived from the measured rotational constants ($\sim 0.34 \text{ amu } \text{\AA}^2$, Table VI). Although the magnitude of the residual in Δ for S_4 is roughly an order of magnitude larger than that for S_3 , it is comparable to that found for the empirical equilibrium structures of other planar molecules of similar size, such as SiC_3 .³⁵

Owing to the difficulties in properly treating electron correlation, previous theoretical studies predicted geometrical parameters of S_4 that are in poor agreement with those derived here. Qualitatively, S_4 can be thought of as two S_2 triplet states in which one of the unpaired electrons of an S_2 fragment is used to make a bond to the other fragment,³⁶ resulting in a substantial amount of biradical character. Inspection of the coupled-cluster wave function for S_4 reveals relatively large double-excitation amplitudes, which is a hallmark of biradical character in species such as ozone and the benzyne. Thus the rather powerful treatment of correlation afforded by the CCSD(T) model provides a good description of the electronic structure of this molecule.

VI. DISCUSSION

Further study of interchange tunneling in S_4 is worthwhile, including a more sophisticated theoretical treatment of the dynamical motion, and observations of rotational spectra in vibrationally excited states, particularly in ν_2 and ν_3 (Fig. 7) which play principal roles in the tunneling coordinate. While the vibrational state dependence of the tunneling splitting in the normal isotopic species of S_4 is of interest, this is even more so for the isotopic forms. The present laboratory study has succeeded in determining the ground-state rotational constants for $^{34}\text{SS}_3$ and S^{34}SSS , but the distinction between these two structures will diminish as the level of vibrational excitation increases, because the two are linked by the low-lying transition state of D_{2h} symmetry. Therefore

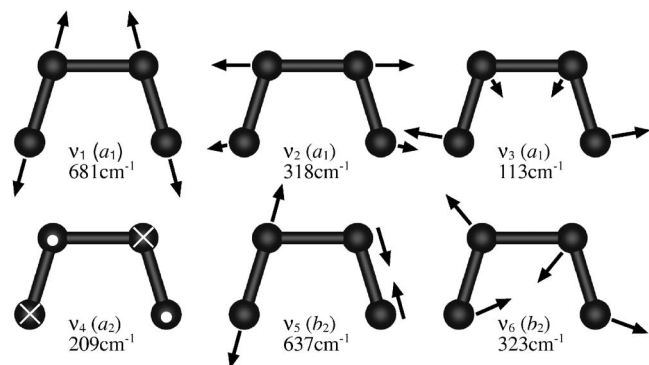


FIG. 7. Normal vibrational modes of S_4 . Fundamental vibrational frequencies calculated at the CCSD(T)/cc-pVTZ level of theory. Length and direction of displacement vectors are approximate.

an investigation of the rotational spectra of isotopically substituted species of S_4 in vibrationally excited states might provide additional insights into the dynamics of this curious molecule. Interchange tunneling could be observed directly in the fully substituted sulfur-33 species because this species obeys Fermi–Dirac statistics and all rotational levels exist; with the present sensitivity this would require an isotopically enriched sample.

The substantial abundances of S_3 and S_4 in our molecular beam suggest that less stable isomers (such as the C_s isomer of S_4 in Fig. 8), and even larger sulfur clusters with more than four atoms may be within reach. Very little is known about the next member in the series S_5 . Its most stable isomer is predicted to be a half-boat structure with C_s symmetry that is moderately polar [0.39 D (Ref. 37)], but fairly floppy, with a low barrier to pseudorotation. For S_6 , the most stable form is predicted to be a nonpolar chair configuration similar to that observed in the solid phase. Less stable isomers of S_6 , and even larger pure sulfur clusters may also be present in our beam.

In addition to pure sulfur clusters, exotic sulfur oxides are of considerable chemical interest. A number of small oxides of sulfur such as S_3O and higher sulfur monoxides S_nO have not been studied by high-resolution spectroscopy, but may be detectable by the same technique used here to characterize the pure sulfur clusters. Both the planar *cis*- and *trans*-isomers of S_3O are polar, unlike isovalent S_4 and S_2O_2 , for which only the *cis*-isomers are polar. Owing to the high reactivity of heated sulfur with oxygen and to the intense rotational lines of S_2O observed in our discharge sources,

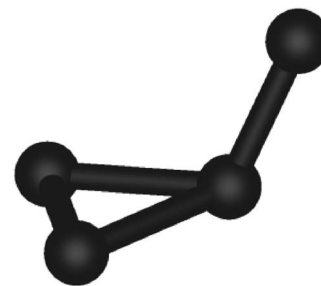


FIG. 8. Molecular structure of a polar C_s isomer of S_4 predicted to lie about 14 kcal/mol higher in energy than the C_{2v} isomer (Ref. 6) shown in Fig. 1.

several of these sulfur oxides are good candidates for detection.

Both S_3 and S_4 are of astronomical interest because sulfur is one of the most cosmically abundant second-row elements, and these are the smallest polar sulfur clusters. Sulfur chemistry in space is not very well understood, primarily because the major reservoir of sulfur has not been identified. Thus detection of S_3 and S_4 might provide important quantitative information on the abundance and form of elemental sulfur. A detailed account of the prospects for observing S_3 and S_4 in Galactic molecular sources has been discussed elsewhere.³⁸ In the solar system, both S_3 and S_4 may be detectable in the Jovian moon Io and in comets, because S and S_2 have been observed at UV wavelengths in these objects. The abundances of many of the 14 sulfur-containing molecules detected in Galactic molecular sources are high in hot dense cores, so S_3 and S_4 are plausible candidates for detection in such objects. The laboratory measurements in the centimeter- and millimeter-wave bands discussed here provide the basic spectroscopic information needed for deep radio astronomical searches of these two fundamental molecules.

ACKNOWLEDGMENTS

We thank W. Klemperer, J. K. G. Watson, H. M. Pickett, H. S. P. Müller, J. Gauss, and J. Hahn for helpful discussions; F. J. Lovas for providing rotational data on the H_2S dimer prior to publication; and E. S. Palmer for laboratory assistance. The work in Cambridge was supported by NASA Grant No. NAG5-9379 and NSF Grant No. AST-9820722. One of the authors (J.F.S.) acknowledges the support of the Robert A. Welch Foundation and the NSF. Another author

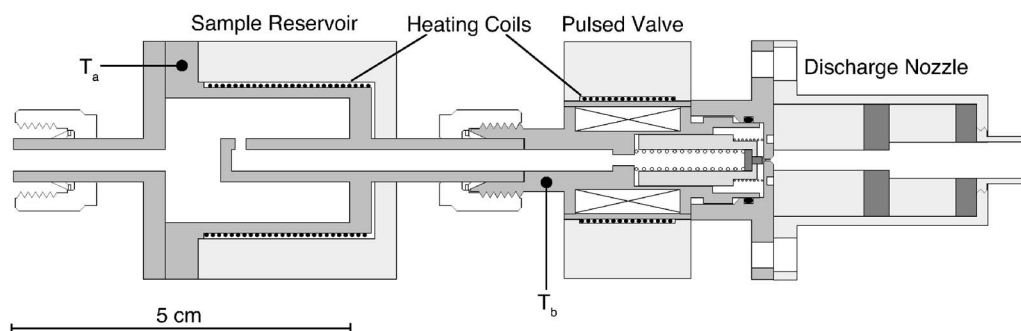


FIG. 9. Cross section of the heated nozzle.

(S.T.) is grateful to the Alexander von Humboldt Foundation for a Feodor Lynen research fellowship.

APPENDIX: THE HEATED NOZZLE

A heated nozzle for low volatile compounds was constructed during the course of the present investigation (Fig. 9). It consists of a sample reservoir which can be resistively heated, a pulsed valve (General valve series 9), and a discharge nozzle similar to that described in Ref. 8. Heating coils (80/20 Nichrome) are wrapped around the sample reservoir and pulsed valve. The coils are enclosed in jackets of Torlon 4203 shown as light shaded areas in Fig. 9. Torlon is a strong machinable thermoplastic that is usable to 260 °C and provides excellent electrical insulation. The sample reservoir and pulsed valve can be heated separately, but the maximum temperature of the entire assembly (200 °C) is limited by the valve.

- ¹B. Eckert and R. Steudel, *Top. Curr. Chem.* **231**, 31 (2003), and references therein.
- ²M. C. McCarthy, S. Thorwirth, C. A. Gottlieb, and P. Thaddeus, *J. Am. Chem. Soc.* **126**, 4096 (2004).
- ³M. C. McCarthy, S. Thorwirth, C. A. Gottlieb, and P. Thaddeus, *J. Chem. Phys.* **121**, 632 (2004).
- ⁴M. W. Wong, *Top. Curr. Chem.* **231**, 1 (2003).
- ⁵G. E. Quelch, H. F. Schaefer III, and C. J. Mardsen, *J. Am. Chem. Soc.* **112**, 8719 (1990).
- ⁶M. W. Wong and R. Steudel, *Chem. Phys. Lett.* **379**, 162 (2003), and references therein.
- ⁷M. C. McCarthy, M. J. Travers, A. Kovács, C. A. Gottlieb, and P. Thaddeus, *Astrophys. J., Suppl. Ser.* **113**, 105 (1997).
- ⁸M. C. McCarthy, W. Chen, M. J. Travers, and P. Thaddeus, *Astrophys. J., Suppl. Ser.* **129**, 611 (2000).
- ⁹S. Yamamoto and S. Saito, *Can. J. Phys.* **72**, 954 (1994); G. Winnewisser, M. Winnewisser, and W. J. Gordy, *J. Chem. Phys.* **49**, 3465 (1968); M. Behnke, dissertation, Universität zu Köln (2001).
- ¹⁰R. L. Brown, *J. Chem. Phys.* **44**, 2827 (1965); R. B. Langford and G. A. Oldershaw, *J. Chem. Soc., Faraday Trans.* **68**, 1550 (1972).
- ¹¹B. Meyer, *Chem. Rev. (Washington, D.C.)* **76**, 367 (1976).
- ¹²R. B. Langford and G. A. Oldershaw, *J. Chem. Soc., Faraday Trans.* **69**, 1389 (1973).
- ¹³The reaction $S(^1D)+OCS \rightarrow S_2+CO$ yields a significant fraction of S_2 in the first electronically excited state [$\hat{a}^1\Delta$; A. J. Hynes, R. C. Richter, A. R. Rosendahl, and C. D. Clark, *Chem. Phys. Lett.* **295**, 25 (1998)], where it cannot readily react to form S_3 (with 1A_1 symmetry), owing to spin and orbital angular momentum restrictions.
- ¹⁴C. A. Gottlieb, P. C. Myers, and P. Thaddeus, *Astrophys. J.* **588**, 655 (2003).
- ¹⁵D. B. Nash, *Icarus* **72**, 1 (1987).
- ¹⁶P. Hassanzadeh and L. Andrews, *J. Phys. Chem.* **96**, 6579 (1992).
- ¹⁷G. D. Brabson, Z. Mielke, and L. Andrews, *J. Phys. Chem.* **95**, 79 (1991).
- ¹⁸Cologne Database for Molecular Spectroscopy, <http://www.cdms.de>; H. S. P. Müller, S. Thorwirth, D. A. Roth, and G. Winnewisser, *Astron. Astrophys.* **370**, L49 (2001).
- ¹⁹R. L. Cook, G. Winnewisser, and D. C. Lindsey, *J. Mol. Spectrosc.* **46**, 276 (1973).
- ²⁰For reviews of coupled-cluster theory, see: T. J. Lee and G. E. Scuseria, in *Quantum Mechanical Electronic Structure Calculations with Chemical Accuracy*, edited by S. R. Langhoff (Kluwer, Dordrecht, 1995); R. J. Bartlett, in *Modern Electronic Structure Theory*, edited by D. R. Yarkony (World Scientific, Singapore, 1995), Pt. II; J. Gauss, in *Encyclopedia of Computational Chemistry*, edited by P. v. R. Schleyer (Wiley, New York, 1998).
- ²¹T. H. Dunning, *J. Chem. Phys.* **90**, 1007 (1989).
- ²²K. Raghavachari, G. W. Trucks, J. A. Pople, and M. Head-Gordon, *Chem. Phys. Lett.* **157**, 479 (1989).
- ²³G. E. Scuseria, *J. Chem. Phys.* **94**, 442 (1991).
- ²⁴J. Gauss and J. F. Stanton, *Chem. Phys. Lett.* **276**, 70 (1997).
- ²⁵J. F. Stanton, C. L. Lopreore, and J. Gauss, *J. Chem. Phys.* **108**, 7190 (1998).
- ²⁶I. M. Mills, in *Modern Spectroscopy: Modern Research*, edited by K. N. Rao and C. W. Matthews (Academic, New York, 1972), pp. 115–140.
- ²⁷J. F. Stanton, J. Gauss, J. D. Watts, W. J. Lauderdale, and R. J. Bartlett, *Int. J. Quantum Chem.* **44**, 879 (1992).
- ²⁸See EPAPS Document No. E-JCPA6-123-009528 for complete lists of experimental transition frequencies. This document can be reached via a direct link in the online article's HTML reference section or via the EPAPS homepage (<http://www.aip.org/pubservs/epaps.html>).
- ²⁹M. E. Sanz, M. C. McCarthy, and P. Thaddeus, *J. Chem. Phys.* **122**, 194319 (2005).
- ³⁰E. Piquenard, O. El Jaroudi, and J. Corset, *J. Raman Spectrosc.* **24**, 11 (1993).
- ³¹L. H. Coudert, K. Matsumura, and F. J. Lovas, *J. Mol. Spectrosc.* **147**, 46 (1991).
- ³²F. Pawłowski, P. Jørgensen, J. Olsen, F. Hegelund, T. Helgaker, J. Gauss, K. L. Bak, and J. F. Stanton, *J. Chem. Phys.* **116**, 6482 (2002).
- ³³J. F. Stanton and J. Gauss, *Int. Rev. Phys. Chem.* **19**, 61 (2000).
- ³⁴The structural optimization at the CCSD(T)/cc-pCVQZ level of theory yields a bond length of 1.913 Å and an angle of 117.54° (J. Gauss, private communication).
- ³⁵J. F. Stanton, J. Gauss, and O. Christiansen, *J. Chem. Phys.* **114**, 2993 (2001).
- ³⁶The binding energy of S_4 (including zero-point vibrational corrections) was calculated at the CCSD(T) level with the cc-pVTZ basis set. The calculation gives a S_2 dimerization enthalpy of -15.3 kcal/mol, implying that the exact value lies within the range of 10–20 kcal/mol. Thus it is not appropriate to view this molecule as a van der Waals complex in spite of the low-energy interchange tunneling mechanism.
- ³⁷S. Millefiori and A. Alparone, *J. Phys. Chem. A* **105**, 9489 (2001).
- ³⁸C. A. Gottlieb, S. Thorwirth, M. C. McCarthy, and P. Thaddeus, *Astrophys. J.* **619**, 939 (2005).